analytical chemistry

pubs.acs.org/ac Article

Immunoprofiling of Severity and Stage of Bacterial Infectious Diseases by Ultrabright Fluorescent Nanosphere-Based Dyad Test Strips

Juanzu Liu, Leping Lin, Peiyu Yao, Wei Zhao, Jiao Hu, Xue-Hui Shi, Shiwu Zhang, Xiaobo Zhu, Dai-Wen Pang, and An-An Liu*

Cite This: *Anal. Chem.* 2022, 94, 8818−8826 Read Online

ACCESS | Metrics & More | Article Recommendations | Supporting Information

ABSTRACT: Bacterial infectious diseases are common clinical diseases that seriously threaten human health, especially in countries and regions with poor environmental hygiene. Due to the lack of characteristic clinical symptoms and signs, it is a challenge to distinguish a bacterial infection from other infections, leading to misdiagnosis and antibiotic overuse. Therefore, there is an urgent need to develop a specific method for detection of bacterial infections. Herein, utilizing ultrabright fluorescent nanospheres (FNs) as reporters, immunochromatographic dyad test strips are developed for the early detection of bacterial infections and distinction of different stages of bacterial infectious diseases in clinical samples. C-reactive protein (CRP) and heparin-binding protein (HBP) are quantified and assayed because their levels in plasma are varied dynamically and asynchronously during the progression of the disease. The detection limits of CRP and HBP can reach as low as 0.51 and 0.65 ng/mL, respectively, due to the superior fluorescence intensity of each FN, which is 570 times stronger than that of a single quantum dot. The assay procedure can be achieved in 22 min, fully meeting the needs of rapid and ultrasensitive detection in the field. This constructed strip has been successfully used to profile the stage and severity of bacterial infections by monitoring the levels of CRP and HBP in human plasma samples, showing great potential as a point-of-care biosensor for clinical diagnosis. In addition to bacterial infections, the developed ultrabright FN-based point-of-care testing can be readily expanded for rapid, quantitative, and ultrasensitive detection of other trace substances in complex systems.

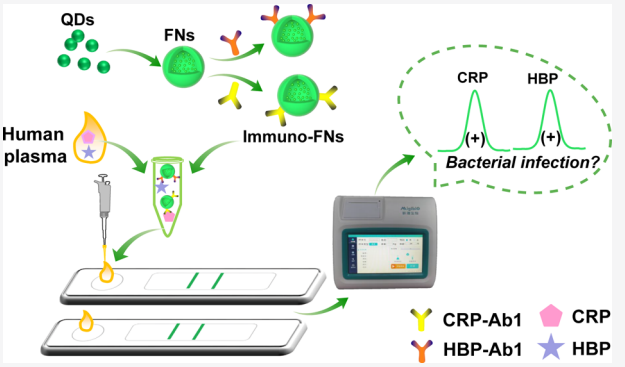

INTRODUCTION

Bacterial infectious diseases caused by pathogenic bacteria are common diseases that severely threaten the health and life of human beings, especially in countries and regions with poor environmental hygiene.[1,2] Therefore, fast and reliable recognition and profiling of bacterial infections are essential in the precise and rational administration.[3] Unfortunately, etiological diagnosis, an acknowledged golden standard for diagnosis of bacterial infectious diseases, is complex and time-consuming, easily resulting in illness aggravation.[4−6] A promising approach to early diagnosis of bacterial infections is an immunological test, including serological tests and antigen detection.[7−9] Because bacterial infections are usually accompanied by inflammation, inflammatory markers, such as C-reactive protein (CRP) and interleukin-6 (IL-6), have been widely used to imply bacterial infectious diseases.[10−12] However, other nonbacterial infections can also induce inflammation, making it impossible to achieve specific diagnosis just by these markers.[13−15] Therefore, utilization of multiple indicators has become a direction of specific diagnosis. For instance, a dual-quantum-dot-labeled lateral flow strip was developed to rapidly quantify procalcitonin (PCT, an indicator of acute bacterial infection)[16,17] and CRP for distinction of inflammation and bacterial and viral infections.[18] Nevertheless, the PCT level in plasma elevates dramatically several hours after acute bacterial infection, which is unable to indicate the early stage of bacterial infection. Additionally, PCT is insusceptible in the cases of chronic and local infections. Heparin-binding protein (HBP), also known as azurocidin, mainly exists in the secretion granules of neutrophils and azoocyan granules.[19] When bacteria invade the body, the activated neutrophils are immediately recruited to the site of infection to release HBP, whose concentration is positively correlated to the severity of infection.[20] Therefore, HBP, together with inflammatory

Received: May 10, 2022
Accepted: May 31, 2022
Published: June 10, 2022

https://doi.org/10.1021/acs.analchem.2c02028
Anal. Chem. 2022, 94, 8818−8826

markers, can serve as a promising indicator combination for early diagnosis, timely treatment, and prognosis of bacterial infection. Given the extremely low HBP level in healthy human plasma (less than 10 ng/mL),[19,21] a highly sensitive method is necessary to detect the trace amount of HBP in complex plasma samples. In addition to the markers, a rapid, sensitive, and portable approach is even more significant in resource-limited areas for diagnosing bacterial infectious diseases.

An immunochromatographic test strip (ICTS), a point-of-care testing (POCT) platform with portability, speediness, cost-effectiveness, and user-friendliness, has been widely used in the detection of metal ions, small molecules, disease markers, and pathogens.[22−25] At present, various materials have been employed as the labels for the ICTS.[26−28] Among them, fluorescent quantum dots (QDs) are one of the most favorable labels because of their high brightness, tunable fluorescence emission, and stability.[29−31] To enhance the sensitivity of POCT, labels with higher brightness have been pursued, aiming at the detection of trace substances in complex systems. QD-based fluorescent nanospheres (FNs) that contain tens of QDs in each FN possess a much stronger fluorescence intensity than that of a single QD.[32−35] More importantly, the optical and colloidal stabilities of FNs can also be improved, which are the prerequisites for the reproducibility of ICTS. Currently, QDs are either embedded in the nanospheres by swelling and emulsion polymerization or coated on the surface of nanospheres by self-assembly and covalent interaction.[36,37] In the former strategies, the QDs are embedded stochastically, leading to heterogeneous fluorescence intensity. In addition, a large number of QDs gathered in one nanosphere may lead to the reduction of fluorescence intensity because of the self-absorption effect.[38] To enhance the fluorescence intensity, in our previous work, FNs are constructed by assembling one or multiple layers of QDs on the surface of polymer nanospheres, which have been used to sensitively detect disease markers (eg. CRP), pathogenic microorganisms (*Salmonella typhimurium* and Ebola virus glycoprotein), and tumor cells.[1,39−41] Although the later strategy can fabricate FNs with stronger fluorescence intensity, the stability of the FNs might be a concern considering the environmental impact and the leak of QDs on the surface. Therefore, an easy-to-fabricate synthetic strategy for FNs with superior brightness and stability is urgent for the development applications of the ICTS.

Herein, ultrabright FNs with photostability are prepared by a double miniemulsion polymerization method. To balance the brightness and stability, the hydrophobic QDs are mixed with monomers before the polymerization, suppressing the oxidation of the QD surface by free radicals during the polymerization process. The fluorescence intensity of each prepared FN is 570 times stronger than that of a single QD. The stable and ultrabright FNs were used as a reporter to develop a POCT for the diagnosis of bacterial infectious diseases. Taking advantage of the combined utilization of CRP and HBP as the markers, the severity and stage of bacterial infections could be profiled rapidly, specifically, and sensitively by ultrabright FN-based dyad test strips in human plasma samples.

EXPERIMENTAL SECTION

Chemicals and Materials. Hydrophobic QDs emitting at 530 nm (QDs_{530}) were purchased from JiaYuan Quantum Dots Co., Ltd. (Wuhan). Isooctyl acrylate, hexadecane, styrene, poly(ethylene glycol) diacrylate (PEGDA), poly(ethylene glycol) methacrylate (PEGMA), sodium dodecyl sulfate (SDS), potassium peroxodisulfate (KPS), poly(acrylic acid) (PAA), and morpholineethanesulfonic acid (MES) were purchased from Shanghai Aladdin Biochemical Technology Co., Ltd. Sodium hydroxide (NaOH) was purchased from Energy Chemical. N-(3-dimethylaminopropyl)-N′-ethylcarbodiimide hydrochloride (EDC) was obtained from Shanghai Medpep Co., Ltd. N-Hydroxysuccinimide (NHS) was bought from Thermo. HBP, mouse anti-HBP antibodies (2H6 for detection (HBP-Ab1) and 1E2 for capture (HBP-Ab2)) were purchased from Biocare Diagnostics Ltd. CRP, rabbit anti-CRP antibodies (R106 for detection (CRP-Ab1), and MM07T for capture (CRP-Ab2)) were purchased from Sino Biological Inc. Goat-antimouse IgG was purchased from Jackson ImmunoResearch Laboratories Inc. Bovine serum albumin (BSA) was purchased from Beijing Solarbio Science & Technology Co., Ltd. Ferroprotein (FER) was obtained from *Escherichia coli*. Goat-antirabbit IgG, heat shock protein 60 (HSP-60), recombinant human CA-125 protein (CA-125), recombinant SARS-CoV-2 spike protein (S1 subunit), and recombinant SARS-CoV-2 nucleocapsid protein were purchased from Beijing Biosynthesis Biotechnology Co., Ltd. Dylight 649-conjugated goat-antimouse IgG and goat-antirabbit IgG were purchased from Abbkine Scientific Co., Ltd. Transferrin human (TRF) and human serum albumin (HSA) were bought from Sigma-Aldrich Co., Ltd. The test strip components were purchased from Shanghai Jieyi Biotechnology Co., Ltd. Ultrapure water (18.2 MΩ·cm) was obtained from a Millipore Milli-Q system and used for the preparation of all buffers.

Synthesis and Charaterization of FNs. QD_{530}-based FNs were prepared by the double miniemulsion polymerization method.[42,43] Briefly, 1 mL of QDs_{530} dispersed in isooctyl acrylate was added into 100 mL of ultrapure water containing SDS and PEGMA (4:1) (used as a surfactant). After stirring for 5 min, the mixture was emulsified by ultrasound to generate miniemulsion A. Similarly, styrene, PEGDA, hexadecane, and ultrapure water were mixed and emulsified to produce miniemulsion B. Subsequently, 20 mL of KPS (1 mg/mL) was added to the double miniemulsion system (a mixture of miniemulsions A and B) in a four-neck flask to initiate the polymerization of styrene into polystyrene (PS). The polymerization reaction was maintained at room temperature for 1 h under an argon atmosphere and further reacted at 70 °C for 16 h. Afterward, the PAA solution was added dropwise. After 12 h, the fabricated QDs/PS nanospheres (FNs) were purified by gradient centrifugation and stored at 4 °C for further use.

The particle concentrations of FNs and hydrophobic QDs_{530} with the same mass concentration (10 mg/mL) were determined by a Zetasizer Ultra (Malvern Panalytical). The fluorescence intensities of the FNs and QDs_{530} (10 pM) were measured using a fluorescence spectrometer (LS 55, Perkin Elmer).

Preparation of Immuno-FNs. Immuno-FNs were fabricated following the previously reported method.[34,39] Typically, EDC and NHS were added into 200 μL of 2 mg/mL FNs (MES buffer, pH = 6.0) at room temperature after stirring for 20 min. After removing excess EDC/NHS by centrifugation, the FNs were resuspended in an equal volume of phosphate buffer and mixed with 5 μL of CRP-Ab1 and HBP-Ab1 (1 mg/mL). After shaking for 2.5 h, the conjugates were blocked with 1% BSA. The mixture was purified by

https://doi.org/10.1021/acs.analchem.2c02028
Anal. Chem. 2022, 94, 8818−8826

centrifugation at least four times, and the as-prepared FNs-CRP-Ab1 and FNs-HBP-Ab1 were stored at 4 °C.

The FNs, FNs-CRP-Ab1, and FNs-HBP-Ab1, were fixed on coverslips by heating and incubated with corresponding Dylight 649-conjugated secondary antibodies (goat-antirabbit IgG and goat-antimouse IgG) for 15 min. After washing with PBS three times, the slides were imaged under a 100× objective mounted on a spinning-disk confocal super-resolution microscope (Olympus IXplore SpinSR10). The fluorescence signals of FNs, FNs-CRP-Ab1, FNs-HBP-Ab1, and Dylight 649-conjugated secondary antibodies (488 nm laser, 525/50 nm emission filter and 635 nm laser, 685/40 nm emission filter) were imaged alternatively onto an sCMOS detector (Prime 95B). The colocalization efficiency was analyzed by ImageJ software.

Construction of the ICTS and Detection of CPR and HBP in a Buffer. A strip is composed of four components: sample pad, nitrocellulose membrane, absorbent pad, and plastic adhesive card. The sample pad is made from glass fiber. The nitrocellulose membrane (Unisart CN 140) was sprayed with CRP-Ab2 or HBP-Ab2 as a test line (TL) and corresponding secondary antibodies as a control line (CL) by a platform precision dispenser (HGS510, AUTOKUN). After being dried at 37 °C for 2 h, the nitrocellulose membrane and other components were assembled on a plastic adhesive card and then cut into 3.9 mm strips by a guillotine cutter (HGS210, AUTOKUN). The strips were stored in a desiccator at 4 °C for further use.

FNs-CRP-Ab1 and FNs-HBP-Ab1 were incubated with different concentrations of CRP (0−2000 ng/mL) and HBP (0−1000 ng/mL) for minutes, respectively. Then, the mixture was loaded onto the sample pad, allowing all running buffers to be absorbed and migrated along the strip. Subsequently, the fluorescence intensity of TL was measured by a quantitative immunofluorescence chromatography reader (FIA688, Guangzhou Magic Biotech Co., Ltd.). Each sample was tested three times, and the error bar was plotted by standard deviation.

Profiling of Human Plasma Samples. The human plasma samples were obtained from volunteers in the Tianjin Union Medical Center. All of the experiments complied with relevant laws and regulations and were approved by the Biomedical Ethics Review Committee of Nankai University. The plasma samples were incubated with immuno-FNs before being tested following the aforementioned procedures. The concentrations of CRP and HBP were calculated by their corresponding calibration curves. Because the level of CRP is generally 2−3 orders of magnitude higher than that of HBP in human plasma, the plasma samples were diluted with a buffer for the determination of CRP.

RESULTS AND DISCUSSION

Mechanism of Ultrabright FN-Based Dyad Test Strips for Immunoprofiling. As mentioned in the Introduction, it is a great challenge to specifically detect bacterial infections by a single marker. A combination of two (or even more) markers whose levels vary dynamically, asynchronously, and apparently in different stages along with the disease development can achieve specific diagnosis and profiling of the stage and severity of infection. According to this rule, CRP and HBP were selected as the biomarkers for bacterial infection in the present work. The HBP level increases rapidly after bacterial infection and falls back at around 6 h postinfection. By contrast, the CRP level typically arises in 6−12 h and peaks at ∼48 h after the inflammatory stimulus, whose concentration is generally proportional to the severity of tissue infection.[45] By quantitatively profiling these two biomarkers simultaneously, the stages of bacterial infection can be indicated, as shown in Scheme 1. The capture and detection antibody pair that are

Scheme 1. Schematic Illustration of Ultrabright FN-Based Dyad Test Strips[a]

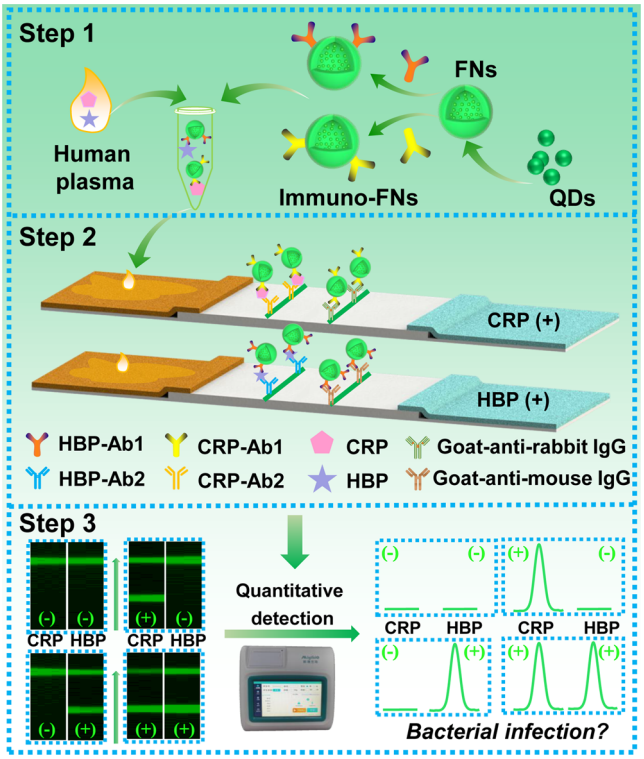

[a]Step 1: synthesis of ultrabright immuno-FNs; step 2: detection schematic of CRP and HBP; step 3: immunoprofiling of bacterial infectious diseases.

loaded on the nitrocellulose membrane and conjugated on the FNs can form a sandwich structure with the corresponding analytes (antigens), leading to the appearance of fluorescence signal on the TL. The fluorescence intensity is dependent on the number of captured antigen-immuno-FN complexes. The free immuno-FNs will be captured by the secondary antibodies loaded on the CL; therefore, a fluorescing CL can guarantee the validation of the strip.

To profile the stage and severity of bacterial infections, the reported CRP/HBP levels in healthy person's plasma are used as the threshold (CRP: 10 μg/mL, HBP: 10 ng/mL) for assessing the testing results.[19,44] When the concentrations of both markers are lower than their thresholds, the subject is healthy (in terms of infection) or has recovered (entitled "infection-free" in this work). The excessive CRP level and normal HBP level represent that the subject is suffering from inflammation or bacterial infection (middle or late stage). And the contrary result represents an early bacterial infection. In the case where both markers are over the thresholds, especially, far exceeded, it can be a severe acute bacterial infection or even more complicated infection that has to be treated immediately.

Physicochemical Properties of Ultrabright FNs and Immuno-FNs. Good physicochemical properties, including

https://doi.org/10.1021/acs.analchem.2c02028
Anal. Chem. 2022, 94, 8818−8826

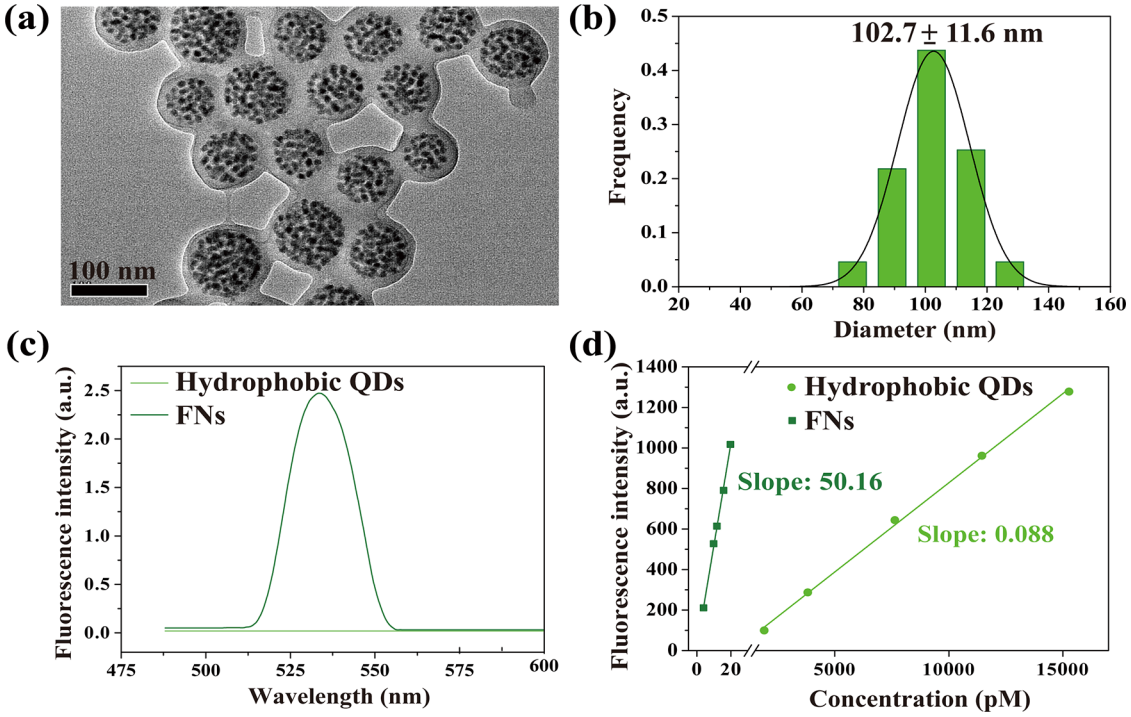

Figure 1. (a) TEM image of FNs, (b) size distribution of FNs, (c) fluorescence spectra of FNs and QDs_{530} at a particle concentration of 10 pM, and (d) linear relationships of the fluorescence intensity vs the particle concentration of FNs and QDs_{530}.

monodispersity, stability, and optical properties of reporters, are the prerequisites for accuracy, reproducibility, and sensitivity of the ICTS. In this work, FNs, served as the reporter, were synthesized by the double miniemulsion polymerization method. As shown in the transmission electron microscopy (TEM) images, the morphology of the FNs, in which tens of QDs_{530} were evenly distributed, was spherical and uniform, with a diameter of ca. 102.7 nm (Figure 1a,b). As aforementioned, the existing approaches to the synthesis of FNs are mostly to prepare polymer nanospheres in advance and then label them with fluorescent materials such as QDs through self-assembling, coating, and embedding. These two-step strategies easily lead to the uneven number and distribution of QDs in each FN. By contrast, the QDs were embedded uniformly into the polymer nanospheres directly during the polymerization procedure in the present work, ensuring the homogeneity, stability, and optical properties of the FNs. The normalized fluorescence spectra of FNs and QDs_{530} were almost overlapped with a very narrow full width at half-maximum (Figures S1 and S2). As for the same particle concentration (10 pM), the fluorescence intensity of FNs is much higher than that of QDs (Figure 1c). The integrated fluorescence intensities of FNs and QDs were plotted against the concentrations. As shown in Figure 1d, the integrated fluorescence intensity of FNs enhanced linearly with the concentration increasing in the range of 3.95×10^{-12}–19.76×10^{-12} M with a slope of 50.16. By contrast, the slope of the plot for QDs was 0.088, indicating that the fluorescence intensity of each FN was ca. 570-fold stronger than that of a single QD_{530}.[39,46] Moreover, the absolute photoluminescence quantum yield (PLQY) of QDs and FNs at the same mass concentration was measured as 94.69% and 95.86%, respectively (Figure S2c,d), demonstrating that the polymerization procedure had negligible effect on the fluorescence properties of QDs. All of these results demonstrated that QDs_{530} were embedded into and dispersed well in each FN, and the structure and optical properties of QDs_{530} were not affected during the double miniemulsion polymerization procedure.

The active group on the surface of the FNs is carboxy, which is necessary for further conjugation. After conjugating with detection antibodies, the hydrodynamic diameter of the resulting FNs-CRP-Ab1 and FNs-HBP-Ab1 in water became 148.7 and 145.3 nm, respectively, which were around 20 nm larger than those of FNs (124.7 nm; Figure 2a–c). The ζ-potential of the FNs increased from −38.6 to −18.2 and −19.8 mV after the conjugation (Figure 2g). In addition, as shown in the confocal fluorescence images, 98.2% of FNs-CRP-Ab1 and 91.4% of FNs-HBP-Ab1 colocalized specifically with their corresponding Dylight 649-conjugated secondary antibodies (Figures 2d–f and S3). The values of intensity correlation quotients (ICQs) are 0.28 and 0.21, indicating strong colocalizations.[47] These results demonstrated that the detection antibodies were successfully conjugated to the surface of FNs with a high labeling efficiency. Such a high efficiency guaranteed the sensitivity of the ICTS, avoiding false-negative results. The fluorescence intensity of the FNs, FNs-CRP-Ab1, and FNs-HBP-Ab1 was stable for months when being stored at 4 °C, which was of great importance to the sensitivity and reproducibility of the ICTS assay (Figure 2h,i).

Evaluation of the Performance of ICTS. The feasibility of the ICTS for detection of CRP and HBP was investigated in the PBS buffer. The signals of immuno-FNs bound nonspecifically on the nitrocellulose membrane including the TL were negligible (Figure S4), avoiding false-positive results. When CRP or HBP existed, fluorescing TLs were observed specifically on their corresponding strips, ensuring the feasibility of the ICTS.

https://doi.org/10.1021/acs.analchem.2c02028
Anal. Chem. 2022, 94, 8818−8826

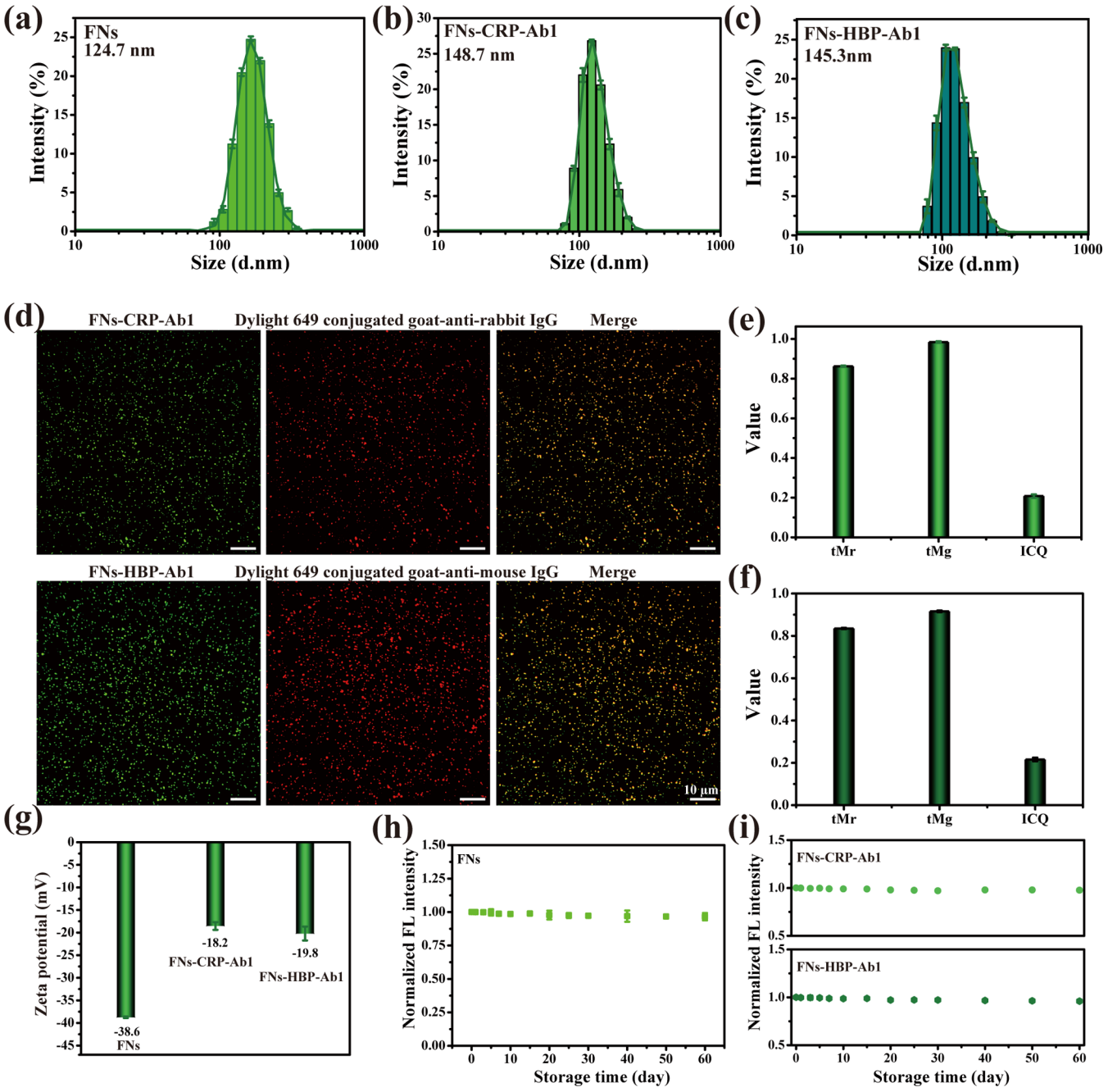

Figure 2. Characterization of FNs, FNs-CRP-Ab1, and FNs-HBP-Ab1. (a−c) Hydrodynamic sizes; (d) colocalization analysis of fluorescence signals between FNs-CRP-Ab1/FNs-HBP-Ab1 and Dylight 649-conjugated goat-antirabbit IgG/goat-antimouse IgG, respectively; (e, f) values of tMg (the percentage of green signals colocalized with red signals in the thresholded images), tMr (the percentage of red signals colocalized with green signals in the thresholded images), and intensity correlation quotient analyzed by ImageJ; (g) ζ-potentials of FNs, FNs-CRP-Ab1, and FNs-HBP-Ab1; and (h, i) fluorescence stability of the FNs, FNs-CRP-Ab1, and FNs-HBP-Ab1 mornitored for 60 days (n = 3).

To obtain optimal performance of the ICTS, the type of running buffer, the concentration of surfactants in the running buffer, and the incubation and running time were optimized successively. First, the running buffers, including ultrapure water, PBS buffer, MES buffer, Britton−Robison (BR) buffer, and Tris buffer, with various ionic strength, pH values, and concentrations of surfactant (generally Tween-20, TW20 for short) were employed to analyze the same sample. The fluorescence signals of the TL, CL, and membrane were used to evaluate the effect of running buffers. Among all of the buffers, PBS containing 1.0% of TW20 was optimal, by which the fluorescence intensity of TL reached the maximum, and the background signal on the membrane was too weak to be detected, affording a good signal-to-background ratio (Figure S5a,b). In addition to the running buffer, the incubation time of immuno-FNs and analyte was optimized as 7 min, which was an important factor affecting the speediness of ICTS (Figure S5c). Using the optimal running buffer, the fluorescence intensity peaked after 15 min migration, generating the optimum outcome (Figure S5d). In a word, the optimal conditions were 7 min incubation and 15 min running in PBS containing 1.0% TW20.

https://doi.org/10.1021/acs.analchem.2c02028
Anal. Chem. 2022, 94, 8818−8826

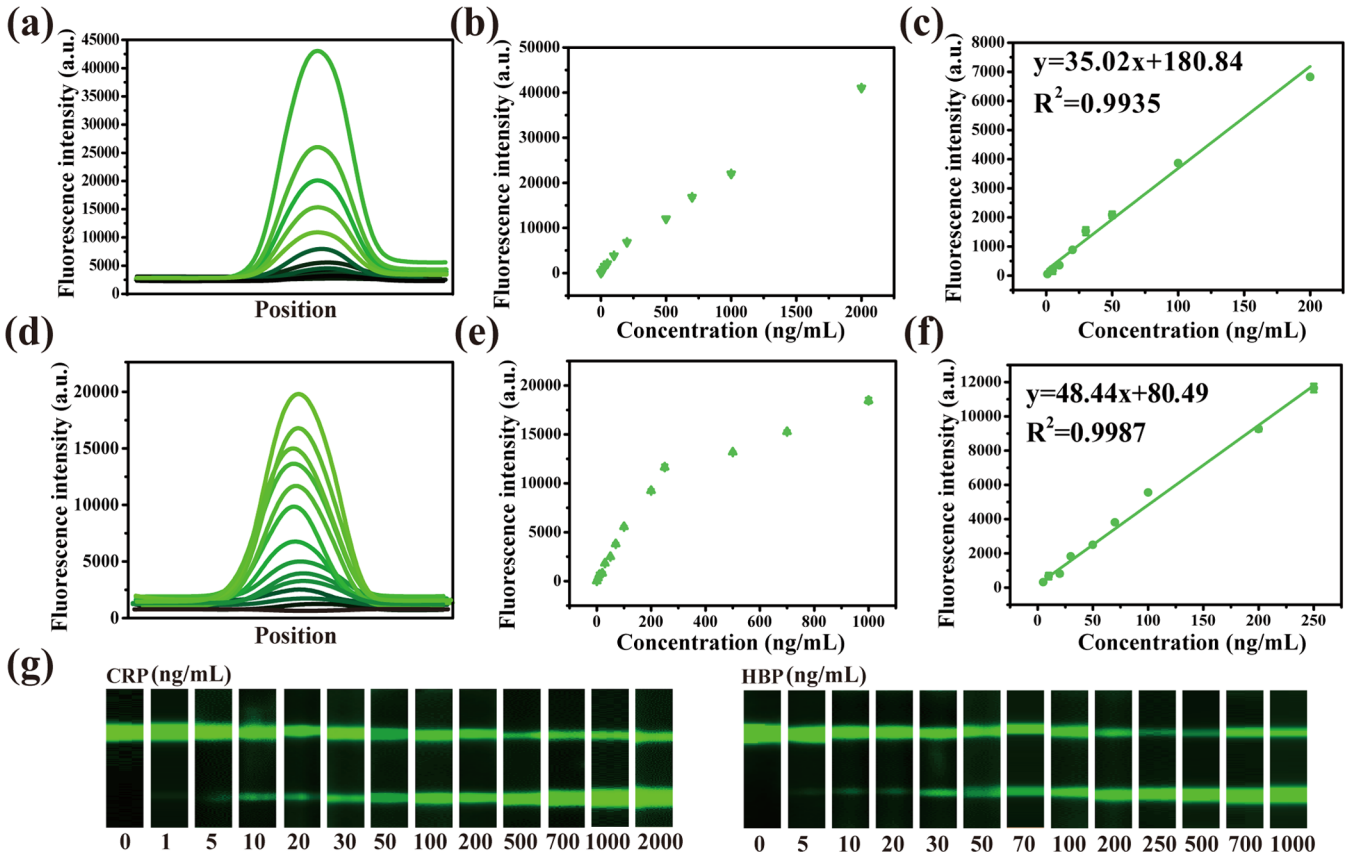

Figure 3. Quantitative detection of CRP and HBP in a buffer. (a) Fluorescence intensities of TLs with different concentrations of CRP in a range of 0−2000 ng/mL (from bottom to top: 0, 1, 5, 10, 20, 30, 50, 100, 200, 500, 700, 1000, 2000 ng/mL). (b) Corresponding scatter plot of the fluorescence intensity as a function of the concentrations of CRP (n = 3). (c) Linear fitting of the fluorescence intensity against the concentration in the range of 1−200 ng/mL of CRP. (d) Fluorescence intensities of TLs with different concentrations of HBP in a range of 0−1000 ng/mL (from bottom to top: 0, 5, 10, 20, 30, 50, 70, 100, 200, 250, 500, 700, 1000 ng/mL). (e) Corresponding scatter plot of the fluorescence intensity as a function of the concentrations for HBP (n = 3). (f) Linear fitting of the fluorescence intensity against the concentration in the range of 5−250 ng/mL of HBP. (g) Images of the ICTS for CRP and HBP in a buffer under UV excitation.

To ensure the optimal performance of the ICTS and avoid the overload of antibodies, the concentrations of capture antibodies (CRP-Ab2 and HBP-Ab2) sprayed on the membrane were optimized as 0.5 and 0.8 mg/mL, respectively (Figure S6).

To further assess the sensitivity of the ICTS, a series of concentrations of CRP and HBP in the range of 0−2000 and 0−1000 ng/mL were tested, respectively, under the optimal conditions. As shown in Figure 3a−f, the fluorescence intensity of the TLs significantly enhanced with the concentration increase of the analytes, exhibiting a good linear relationship in the range of 1−200 ng/mL for CRP and 5−250 ng/mL for HBP (R_{CRP}^2 = 0.9935, R_{HBP}^2 = 0.9987). As a result, the limits of detection (LODs) of CRP and HBP were calculated as 0.51 and 0.65 ng/mL according to the 3σ/slope rule, respectively. Such low detection limits guaranteed their application in the early sensitive detection of CRP and HBP in clinical samples. Figure 3g shows the corresponding images of test strips under UV illumination.

Another prerequisite for clinical sample testing is the anti-interference ability, considering the complicated composition of clinical samples. To this end, common proteins and potential interfering substances in human plasma, such as HSA, FER, TRF, HSP-60, CA-125, SARS-CoV-2 spike protein (S1 subunit), and SARS-CoV-2 nucleocapsid protein, were supplemented in the PBS buffer. Even at an extremely high concentration (1000-fold higher than that of CRP and HBP), these substances induced very weak fluorescence signals on the TLs, which were less than one-tenth of those produced by CRP/HBP (Figures 4a and S7), demonstrating that the ICTS possessed a strong anti-interference ability, and were suitable for the clinical sample testing.

Profiling of Stage and Severity of Bacterial Infections in Human Plasma Samples. As aforementioned, the thresholds for assessing the bacterial infections were set as 10 μg/mL for CRP and 10 ng/mL for HBP. Therefore, quantitative analysis of these two biomarkers in the human plasma samples is the core of this strategy. To quantitatively analyze their concentrations, the calibration curves were plotted by measuring the human plasma that was supplemented with different concentrations of CRP (1−100 ng/mL) and HBP (5−200 ng/mL) (Figure 4b−e). Subsequently, the levels of CRP and HBP in 15 patients' plasma were evaluated by the ICTS according to these calibration curves and further profiled to judge the bacterial infection (Figure 4f and Table 1). As shown in Table 1, the testing results of the plasma samples are highly consistent with those measured by the medical blood routine test (CRP) and a commercial kit aiming at the detection of HBP, indicating that the ICTS is a reliable method for the detection of CRP and HBP. Because of the high sensitivity, a trace amount of HBP (less than 1 ng/mL) in human plasma samples can also be detected, as shown in

https://doi.org/10.1021/acs.analchem.2c02028
Anal. Chem. 2022, 94, 8818−8826

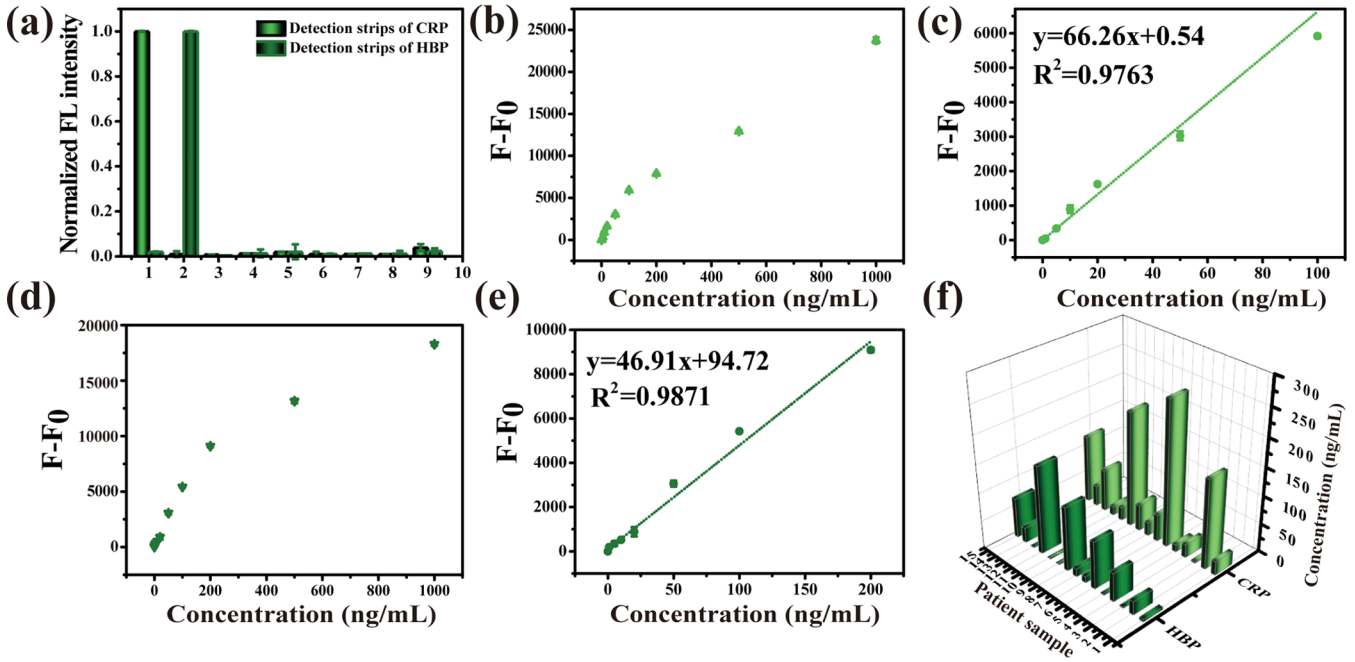

Figure 4. (a) Histograms of the detected fluorescence intensity using different interfering substances for analysis of the detection specificity. The concentrations of CRP and HBP are 100 ng/mL, and the interfering substances are 100 μg/mL (1: CRP; 2: HBP; 3: HSA; 4: FER; 5: TRF; 6: HSP-60; 7: CA-125; 8: SARS-CoV-2 spike protein (S1 subunit); 9: SARS-CoV-2 nucleocapsid protein). (b) Scatter plot of the fluorescence intensity and the amount of CRP with increasing concentrations (0−1000 ng/mL, n = 3) in human plasma. (c) Linear relationship between the fluorescence intensity and the amount of CRP (1−100 ng/mL) in human plasma. F and F_0 are the fluorescence signals in the addition and no addition of CRP, respectively. (d) Scatter plot of the fluorescence intensity and the amount of HBP with increasing concentrations (0−1000 ng/mL, n = 3) in human plasma. (e) Linear relationship between the fluorescence intensity and the amount of HBP (5−200 ng/mL) in human plasma. F and F_0 are the fluorescence signals in the addition and no addition of HBP, respectively. (f) Detection results of the clinical plasma samples with the ICTS (n = 3).

Table 1. Profiling of Bacterial Infectious Diseases in Human Plasma Samples

samples	CRP[a]	SD[b]	CRP[c]	HBP[a]	SD[b]	HBP[d]	qualitative judgment[e]	severity
1	24.45	0.88	24.6	4.45	0.18	4.03	inflammation	mild
2	158.78	0.12	157.9	23.88	0.42	22.62	*	severe
3	2.96	0.92	2.9	1.58	0.02	1.64	−	infection-free
4	23.55	1.15	/	50.55	3.99	52.92	*	moderate
5	12.85	0.39	12.3	0.85	0.20	0.00	indetermination	
6	256.93	7.78	256.9	83.93	2.45	81.88	*	severe
7	48.08	0.58	48.5	11.08	3.37	11.12	inflammation	mild
8	23.43	1.10	/	13.95	1.40	13.17	inflammation	mild
9	46.78	2.23	46.8	113.08	7.03	115.37	*	severe
10	203.25	1.52	204.5	0.43	0.50	0.12	inflammation	severe
11	21.60	0.81	21.5	0.00	0.00	0.20	inflammation	mild
12	15.88	1.24	/	155.78	7.00	152.28	*	severe
13	75.11	2.38	75.2	1.35	3.33	1.11	inflammation	moderate
14	36.69	1.03	/	25.62	1.99	26.72	*	moderate
15	120.91	5.49	/	70.91	1.49	71.04	*	severe

[a]Values represent the detection results of CRP and HBP by ICTS. [b]Values represent the standard deviation of parallel results (n = 3). [c]Values represent the detection result of CRP in a hospital blood routine, / represents that the value is unavailable. [d]Values represent the detection result of HBP by the commercial kit (CRP: μg/mL, HBP: ng/mL). [e]* represents the person is suffering from bacterial infection; − represents the person is uninfected by bacteria.

samples 5, 10, and 11. Among them, the CRP level in sample 5 slightly exceeded the threshold, which needs further assessment. According to the threshold for CRP (10 μg/mL), only sample 3 was CRP negative, in which the HBP was also negative, indicating that this volunteer was infection-free. Among the CRP-positive samples, 7 of 14 samples (2, 4, 6, 9, 11, 14, and 15) were judged as a bacterial infection because the level of HBP is over 10 ng/mL. In samples 7 and 8, the levels of CRP exceeded 20 μg/mL, which were considered as a mild infection; however, the HBP levels exceeded the threshold slightly, and a further assay was needed for the diagnosis of bacterial infection. The severity of the inflammation and the bacterial infection is positively correlated with the level of HBP and CRP. In the case that the level of HBP exceeds the threshold, if the level of CRP in human plasma increases to 20−50 mg/L, it can be considered as a mild infection, and the

https://doi.org/10.1021/acs.analchem.2c02028
Anal. Chem. 2022, 94, 8818−8826

bacterial infections can be improved spontaneously by the immune system. When the CRP content increases to 60−120 mg/L, bacterial infections are moderate, needing treatment. Once the level of CRP increases to 120 mg/L or higher, it will be considered a severe, bacteremic, or septic infection. [47] Hence, the severity of the patient could also be assessed from the quantitative results, which would be significant to assist doctors in diagnosing and prescribing.[20,44,48,49] The other five samples demonstrated the infection induced by other reasons except for the bacteria. All of these results indicated that this ultrabright FN-based ICTS strategy is a promising method for point-of-care testing of inflammation and bacterial infection. More importantly, this strategy can be used as a model for rapid, quantitative, and ultrasensitive detection of other trace substances in complex systems.

CONCLUSIONS

In summary, ultrabright FN-based dyad test strips were developed for immunoprofiling of severity and stage of bacterial infectious diseases by quantitatively assaying the levels of CRP and HBP in human plasma. Benefiting from the excellent physicochemical properties of the FNs, the ICTS biosensor can recognize a trace of markers (0.51 and 0.65 ng/mL for CRP and HBP, respectively) within 22 min. Moreover, the biosensor exhibits high specificity, strong anti-interference ability, and good reproducibility in a complex system (human plasma). The testing results of the plasma samples are highly consistent with a blood routine test and commercial kit. This strategy provides guidance for medication and anticipation of developing trends. By alternating the captor conjugated on the FNs, this biosensor is promising to be developed into a universal household and onsite application kit for quantitative analysis of various trace substances in complex systems in the field of medicine, veterinary sciences, food science, and environmental science.

ASSOCIATED CONTENT

Supporting Information

The Supporting Information is available free of charge at https://pubs.acs.org/doi/10.1021/acs.analchem.2c02028.

Fluorescence emission spectrum, absorption spectrum, TEM image, size distribution, and the hydrodynamic size of QDs (Figure S1); absorption spectrum, fluorescence emission spectrum of FNs, and absolute PLQY of QDs and FNs (Figure S2); confocal images of FNs and Dylight 649-conjugated goat-antirabbit IgG/Dylight 649-conjugated goat-antimouse IgG (Figure S3); fluorescence signal changes and images of the ultrabright FN-based dyad ICTS feasibility analysis (Figure S4); optimization of the experimental conditions (Figure S5); optimization of capture antibodies concentration on TLs (Figure S6); and photos of the ICTS with different interfering substances (Figure S7) (PDF)

AUTHOR INFORMATION

Corresponding Author

An-An Liu − *State Key Laboratory of Medicinal Chemical Biology, Tianjin Key Laboratory of Biosensing and Molecular Recognition, Frontiers Science Center for New Organic Matter, Research Center for Analytical Sciences, College of Chemistry, Frontiers Science Center for Cell Responses, Haihe Laboratory of Sustainable Chemical Transformations, Nankai University, Tianjin 300071, P. R. China;* orcid.org/0000-0002-3563-6290; Email: ananliu@nankai.edu.cn

Authors

Juanzu Liu − *State Key Laboratory of Medicinal Chemical Biology, Tianjin Key Laboratory of Biosensing and Molecular Recognition, Frontiers Science Center for New Organic Matter, Research Center for Analytical Sciences, College of Chemistry, Frontiers Science Center for Cell Responses, Haihe Laboratory of Sustainable Chemical Transformations, Nankai University, Tianjin 300071, P. R. China*

Leping Lin − *State Key Laboratory of Medicinal Chemical Biology, Tianjin Key Laboratory of Biosensing and Molecular Recognition, Frontiers Science Center for New Organic Matter, Research Center for Analytical Sciences, College of Chemistry, Frontiers Science Center for Cell Responses, Haihe Laboratory of Sustainable Chemical Transformations, Nankai University, Tianjin 300071, P. R. China; Wuhan Jiayuan Quantum Dots Co., Ltd., Wuhan 430074, P. R. China*

Peiyu Yao − *Department of Emergency, Department of Pathology, Tianjin Union Medical Center, Tianjin 300121, P. R. China*

Wei Zhao − *State Key Laboratory of Medicinal Chemical Biology, Tianjin Key Laboratory of Biosensing and Molecular Recognition, Frontiers Science Center for New Organic Matter, Research Center for Analytical Sciences, College of Chemistry, Frontiers Science Center for Cell Responses, Haihe Laboratory of Sustainable Chemical Transformations, Nankai University, Tianjin 300071, P. R. China*

Jiao Hu − *Hubei Key Laboratory of Environmental and Health Effects of Persistent Toxic Substances, School of Environment and Health, Jianghan University, Wuhan 430056, P. R. China;* orcid.org/0000-0002-3796-5098

Xue-Hui Shi − *State Key Laboratory of Medicinal Chemical Biology, Tianjin Key Laboratory of Biosensing and Molecular Recognition, Frontiers Science Center for New Organic Matter, Research Center for Analytical Sciences, College of Chemistry, Frontiers Science Center for Cell Responses, Haihe Laboratory of Sustainable Chemical Transformations, Nankai University, Tianjin 300071, P. R. China*

Shiwu Zhang − *Department of Emergency, Department of Pathology, Tianjin Union Medical Center, Tianjin 300121, P. R. China*

Xiaobo Zhu − *Wuhan Jiayuan Quantum Dots Co., Ltd., Wuhan 430074, P. R. China*

Dai-Wen Pang − *State Key Laboratory of Medicinal Chemical Biology, Tianjin Key Laboratory of Biosensing and Molecular Recognition, Frontiers Science Center for New Organic Matter, Research Center for Analytical Sciences, College of Chemistry, Frontiers Science Center for Cell Responses, Haihe Laboratory of Sustainable Chemical Transformations, Nankai University, Tianjin 300071, P. R. China;* orcid.org/0000-0002-7017-5725

Complete contact information is available at: https://pubs.acs.org/10.1021/acs.analchem.2c02028

Notes

The authors declare no competing financial interest.

https://doi.org/10.1021/acs.analchem.2c02028
Anal. Chem. 2022, 94, 8818−8826

■ ACKNOWLEDGMENTS

This work was supported by the National Key R&D Program of China (2019YFA0210100), the "Frontiers Science Center for New Organic Matter", Nankai University (63181206), "the Fundamental Research Funds for the Central Universities", Nankai University (63201024), Tianjin Natural Science Foundation (19JCQNJC02400), and the Haihe Laboratory of Sustainable Chemical Transformations.

■ REFERENCES

(1) Hu, J.; Jiang, Y. Z.; Tang, M.; Wu, L. L.; Xie, H. Y.; Zhang, Z. L.; Pang, D. W. *Anal. Chem.* **2019**, *91*, 1178−1184.
(2) Huang, Y.; Chen, W.; Chung, J.; Yin, J.; Yoon, J. *Chem. Soc. Rev.* **2021**, *50*, 7725−7744.
(3) Wen, C. Y.; Hu, J.; Zhang, Z. L.; Tian, Z. Q.; Ou, G. P.; Liao, Y. L.; Li, Y.; Xie, M.; Sun, Z. Y.; Pang, D. W. *Anal. Chem.* **2013**, *85*, 1223−1230.
(4) Deusenbery, C.; Wang, Y.; Shukla, A. *ACS Infect. Dis.* **2021**, *7*, 695−720.
(5) Lagier, J. C.; Edouard, S.; Pagnier, I.; Mediannikov, O.; Drancourt, M.; Raoult, D. *Clin. Microbiol. Rev.* **2015**, *28*, 208−236.
(6) Váradi, L.; Luo, J. L.; Hibbs, D. E.; Perry, J. D.; Anderson, R. J.; Orenga, S.; Groundwater, P. W. *Chem. Soc. Rev.* **2017**, *46*, 4818−4832.
(7) Wen, C. Y.; Jiang, Y. Z.; Li, X. Y.; Tang, M.; Wu, L. L.; Hu, J.; Pang, D. W.; Zeng, J. B. *ACS Appl. Mater. Interfaces* **2017**, *9*, 9416−9425.
(8) Zhu, Y.; Jovic, M.; Lesch, A.; Tissieres Lovey, L.; Prudent, M.; Pick, H.; Girault, H. H. *Angew. Chem., Int. Ed.* **2018**, *57*, 14942−14946.
(9) Gollan, B.; Grabe, G.; Michaux, C.; Helaine, S. *Annu. Rev. Microbiol.* **2019**, *73*, 359−385.
(10) Plesko, M.; Suvada, J.; Makohusova, M.; Waczulikova, I.; Behulova, D.; Vasilenkova, A.; Vargova, M.; Stecova, A.; Kaiserova, E.; Kolenova, A. *Neoplasma* **2016**, *63*, 752−760.
(11) Olivares, M.; Richardson, M. W.; Visintainer, P. *Blood* **2013**, *122*, 4682.
(12) Kaw, M.; Singh, S. *Gastrointest. Endosc.* **2001**, *54*, 435−440.
(13) Quarck, R.; Nawrot, T.; Meyns, B.; Delcroix, M. *J. Am. Coll. Cardiol.* **2009**, *53*, 1211−1218.
(14) Fishman, D.; Faulds, G.; Jeffery, R.; Mohamed-Ali, V.; Yudkin, J. S.; Humphries, S.; Woo, P. *Clin. Invest.* **1998**, *102*, 1369−1376.
(15) Tsao, Y. T.; Tsai, Y. H.; Liao, W. T.; Shen, C. J.; Shen, C. F.; Cheng, C. M. *Trends Mol. Med.* **2020**, *26*, 1118−1132.
(16) Chan, Y. L.; Tseng, C. P.; Tsay, P. K.; Chang, S. S.; Chiu, T. F.; Chen, J. C. *Crit. Care* **2004**, *8*, R12−R20.
(17) Memar, M. Y.; Varshochi, M.; Shokouhi, B.; Asgharzadeh, M.; Kafil, H. S. *Biomed. Pharmacother.* **2017**, *96*, 936−943.
(18) Qi, X.; Huang, Y.; Lin, Z.; Xu, L.; Yu, H. *Nanoscale Res. Lett.* **2016**, *11*, 167.
(19) Linder, A.; Arnold, R.; Boyd, J. H.; Zindovic, M.; Zindovic, I.; Lange, A.; Paulsson, M.; Nyberg, P.; Russell, J. A.; Pritchard, D.; Christensson, B.; Akesson, P. *Crit. Care Med.* **2015**, *43*, 2378−2386.
(20) Linder, A.; Soehnlein, O.; Akesson, P. *J. Innate Immun.* **2010**, *2*, 431−438.
(21) Yang, Y.; Liu, G.; He, Q.; Shen, J.; Xu, L.; Zhu, P.; Zhao, M. *J. Immunol. Res.* **2019**, *2019*, No. 7515346.
(22) Wu, Y.; Zhou, Y.; Leng, Y.; Lai, W.; Huang, X.; Xiong, Y. *Biosens. Bioelectron.* **2020**, *157*, No. 112168.
(23) Ji, T.; Xu, X.; Wang, X.; Cao, N.; Han, X.; Wang, M.; Chen, B.; Lin, Z.; Jia, H.; Deng, M.; Xia, Y.; Guo, X.; Lei, M.; Liu, Z.; Zhou, Q.; Chen, G. *ACS Nano* **2020**, *14*, 16864−16874.
(24) Jauset-Rubio, M.; Tomaso, H.; El-Shahawi, M. S.; Bashammakh, A. S.; Al-Youbi, A. O.; O'Sullivan, C. K. *Anal. Chem.* **2018**, *90*, 12745−12751.
(25) Brangel, P.; Sobarzo, A.; Parolo, C.; Miller, B. S.; Howes, P. D.; Gelkop, S.; Lutwama, J. J.; Dye, J. M.; McKendry, R. A.; Lobel, L.; Stevens, M. M. *ACS Nano* **2018**, *12*, 63−73.
(26) Huang, X.; Aguilar, Z. P.; Xu, H.; Lai, W.; Xiong, Y. *Biosens. Bioelectron.* **2016**, *75*, 166−180.
(27) Wang, L.; Wang, X.; Cheng, L.; Ding, S.; Wang, G.; Choo, J.; Chen, L. *Biosens. Bioelectron.* **2021**, *189*, No. 113360.
(28) Matsumura, Y.; Enomoto, Y.; Takahashi, M.; Maenosono, S. *ACS Appl. Mater. Interfaces* **2018**, *10*, 31977−31987.
(29) Zhang, Q.; Fang, L.; Jia, B.; Long, N.; Shi, L.; Zhou, L.; Zhao, H.; Kong, W. *TrAC, Trends Anal. Chem.* **2021**, *144*, No. 116427.
(30) Taranova, N. A.; Berlina, A. N.; Zherdev, A. V.; Dzantiev, B. B. *Biosens. Bioelectron.* **2015**, *63*, 255−261.
(31) Wang, C.; Hou, F.; Ma, Y. *Biosens. Bioelectron.* **2015**, *68*, 156−162.
(32) Xie, H. Y.; Zuo, C.; Liu, Y.; Zhang, Z. L.; Pang, D. W.; Li, X. L.; Gong, J. P.; Dickinson, C.; Zhou, W. *Small* **2005**, *1*, 506−509.
(33) Song, E. Q.; Wang, G. P.; Xie, H. Y.; Zhang, Z. L.; Hu, J.; Peng, J.; Wu, D. C.; Shi, Y. B.; Pang, D. W. *Clin. Chem.* **2007**, *53*, 2177−2185.
(34) Hu, J.; Wen, C. Y.; Zhang, Z. L.; Xie, M.; Hu, J.; Wu, M.; Pang, D. W. *Anal. Chem.* **2013**, *85*, 11929−11935.
(35) Yang, J.; Lin, Z. Z.; Huang, Z. Y. *Mar. Pollut. Bull.* **2020**, *151*, No. 110812.
(36) Xie, H. Y.; Xie, M.; Zhang, Z. L.; Long, Y. M.; Liu, X.; Tang, M. L.; Pang, D. W.; Tan, Z.; Dickinson, C.; Zhou, W. Z. *Bioconjugate Chem.* **2007**, *18*, 1749−1755.
(37) Song, E. Q.; Hu, J.; Wen, C. Y.; Tian, Z. Q.; Yu, X.; Zhang, Z. L.; Shi, Y. B.; Pang, D. W. *ACS Nano* **2011**, *5*, 761−770.
(38) Wen, C. Y.; Xie, H. Y.; Zhang, Z. L.; Wu, L. L.; Hu, J.; Tang, M.; Wu, M.; Pang, D. W. *Nanoscale* **2016**, *8*, 12406−12429.
(39) Hu, J.; Zhang, Z. L.; Wen, C. Y.; Tang, M.; Wu, L. L.; Liu, C.; Zhu, L.; Pang, D. W. *Anal. Chem.* **2016**, *88*, 6577−6584.
(40) Hu, J.; Jiang, Y. Z.; Wu, L. L.; Wu, Z.; Bi, Y.; Wong, G.; Qiu, X.; Chen, J.; Pang, D. W.; Zhang, Z. L. *Anal. Chem.* **2017**, *89*, 13105−13111.
(41) Wu, L. L.; Zhang, Z. L.; Tang, M.; Zhu, D. L.; Dong, X. J.; Hu, J.; Qi, C. B.; Tang, H. W.; Pang, D. W. *Angew. Chem., Int. Ed.* **2020**, *59*, 11240−11244.
(42) Zhao, Y.; Liu, J.; Chen, Z.; Zhu, X.; Moller, M. *Nat. Commun.* **2018**, *9*, No. 1918.
(43) Xu, H.; Cui, L. L.; Tong, N. H.; Gu, H. C. *J. Am. Chem. Soc.* **2006**, *128*, 15582−15583.
(44) Allin, K. H.; Nordestgaard, B. G. *Crit. Rev. Clin. Lab. Sci.* **2011**, *48*, 155−170.
(45) Li, Q.; Lau, A.; Morris, T. J.; Guo, L.; Fordyce, C. B.; Stanley, E. F. *J. Neurosci.* **2004**, *24*, 4070−4081.
(46) Liu, C.; Bao, L.; Tang, B.; Zhao, J. Y.; Zhang, Z. L.; Xiong, L. H.; Hu, J.; Wu, L. L.; Pang, D. W. *Small* **2016**, *12*, 4702−4706.
(47) Korppi, M. *Acta Paediatr.* **2021**, *110*, 1090−1091.
(48) Dankiewicz, J.; Linder, A.; Annborn, M.; Rundgren, M.; Friberg, H. *Resuscitation* **2013**, *84*, 935−939.
(49) van der Geest, P. J.; Mohseni, M.; Linssen, J.; Duran, S.; de Jonge, R.; Groeneveld, A. B. *Crit. Care* **2016**, *20*, 180.

https://doi.org/10.1021/acs.analchem.2c02028
Anal. Chem. 2022, 94, 8818−8826